Advanced Materials

ADVANCED MATERIALS
www.advmat.de

RESEARCH ARTICLE

Fatigue Resistant Hydrogels Engineered With Twisting Hierarchical Structures

Yinghui Feng[1,2] | Yafei Wang[1] | Chang Wang[1] | Xingmei Chen[1] | Liangjie Shan[1] | Runyi Yan[1] | Zongbao Wang[3] | Sicong Liu[4] | Ji Liu[1]

[1]Department of Mechanical and Energy Engineering, Southern University of Science and Technology, Shenzhen, China | [2]Xiangya School of Pharmaceutical Sciences, Central South University, Changsha, Hunan, China | [3]School of Materials Science and Chemical Engineering, Ningbo University, Ningbo, China | [4]Sino-German College of Intelligent Manufacturing, Shenzhen Technology University, Shenzhen, Guangdong, China

Correspondence: Ji Liu (liuj9@sustech.edu.cn)

Received: 13 November 2025 | **Revised:** 11 February 2026 | **Accepted:** 11 February 2026

Keywords: bioinspired | fatigue resistance | hierarchical structure | hydrogels | twisting

ABSTRACT

Hydrogels hold significant potential for soft robotics and biomedical applications due to their high-water content, tissue-like softness, and biocompatibility, yet their practical utility remains limited by poor fatigue resistance during long-term dynamic loading. Here, we present a twisting strategy that enhances hydrogel materials' mechanical durability through bioinspired torsion methodology, enabling efficient load transfer and energy dissipation. The resulting fibers exhibit improved tensile strength, stretchability, and unprecedented fatigue thresholds while maintaining structural integrity across prolonged cycling. Our strategy is also compatible with various hydrogel systems including poly(vinyl alcohol), alginate, cellulose and corresponding composite systems. This approach benefits from multiscale simulations, revealing that moderate twisting promotes uniform stress distribution through inter-fiber sliding, while excessive twisting causes geometric locking. Proof-of-concept demonstrations include a frog-tongue-inspired actuator showing rapid yet reversible motion under high-frequency cycling, highlighting its exceptional fatigue tolerance. This bioinspired architecture establishes a universal design paradigm for fatigue-resistant hydrogel systems, unlocking their potential in demanding applications from implantable medical devices to adaptive soft robotics.

1 | Introduction

Hydrogels have emerged as a transformative class of soft materials with demonstrated versatility across wearable electronics [1], soft robotics [2], tissue engineering [3, 4], and implantable medical devices [5–7], leveraging their unique combination of high-water content (<80%), tissue-like compliance (Young's modulus of hundreds kPa), intrinsic softness and biocompatibility [8, 9]. While conventional hydrogels can be engineered to exhibit exceptionally high toughness (e.g., <10 000 J m^{-2}) through the incorporation of energy-dissipating moieties, these systems exhibit critical limitations under sustained mechanical loading, specifically, progressive network disassociation reduces their fatigue thresholds (i.e., minimum energy required for fatigue crack propagation) below 50 J m^{-2} [9, 10]. This fundamental disparity between static toughness and cyclic-loading resilience severely constrains their deployment in applications requiring long-term mechanical fidelity, such as load-bearing biomedical implants (e.g., cardiac valves and neural probes) [3, 11], ingestible devices, [6] durable flexible electronics (e.g., strain sensors) [12],

Yinghui Feng and Yafei Wang contributed equally to this work.

and sustainable energy systems (e.g., battery electrolytes) [13, 14]. Natural biological systems like tendons and mussel byssus employ hierarchical architectures with energy dissipation mechanisms to achieve exceptional mechanical robustness, inspiring synthetic hydrogel designs that integrate multi-length-scale structural engineering for improved mechanics [9]. Representative strategies include double-network architectures that distribute mechanical stress between stiff and ductile phases [15, 16], and incorporation of high-energy domains (i.e. nanocrystals and nano/micro fibers) [4, 17–19], in order to mitigate stress concentration and arrest crack propagation. Additional approaches, such as entropy-driven polymer rearrangement and strain-adaptive reinforcement [20–22], have also been employed to extend hydrogel lifespans for dynamic scenarios. These innovations have enabled hydrogel systems to withstand over millions loading cycles, increasing their fatigue threshold by two to three orders of magnitude [2, 23]. However, the fabrication of hydrogel materials with hierarchical structures across multiple length scales remains a significant challenge, constraining the translation of hydrogel innovations from laboratory prototypes to real-world functional materials.

To address these challenges, recent efforts have been dedicated to mimicking nature's approach for structural optimization through controlled polymer chain alignment and anisotropic architecture design, mimicking the prototypes of natural muscles [9, 24]. This biomimetic paradigm has motivated the development of hydrogel networks with hierarchical alignment across multiple length scales [18, 25], enabling efficient stress distribution, enhanced energy dissipation, and crack propagation resistance, thus collectively contributing to exceptional toughness and fatigue resistance [2, 12, 23, 26, 27]. Among these structural configurations, twisted fiber architectures have shown particular promise by enabling multiscale load redistribution through helical alignment mechanisms [28, 29]. Recent studies have demonstrated the effectiveness of such architectures in hydrogel fibers, artificial spider silks, elastocaloric systems, hierarchical composites, and helical lattice metamaterials, achieving simultaneous enhancement in strength, toughness, energy dissipation, and cyclic durability [7, 13, 18, 19, 25, 30–32]. Such enhancement is achieved through three synergistic effects: cooperative stress transfer minimizing local stress concentrations, energy dissipation via inter-/intra-fiber friction during deformation, and crack path tortuosity that enhances defect tolerance [33, 34]. These combined attributes position twisted hydrogel fibers as versatile candidates for load-bearing biomedical composites and engineered soft materials, including artificial spider silk sutures and tendon/ligament-mimetic fiber assemblies [7, 25, 28].

Building on these principles, we present a versatile fabrication strategy for twisted hydrogel fibers that addresses the intrinsic mechanical limitations of conventional hydrogel systems (Figure 1). Through precision control of torsion parameters during the twisting process, we demonstrate substantial enhancements in tensile strain (>200% improvement), fracture toughness (>150% increase), and fatigue resistance (>1000% increase). The developed methodology establishes a generalizable framework for imparting unprecedented fatigue resistance of conventional polymer hydrogel networks, representing a significant advancement in functional material design.

2 | Results and discussion

2.1 | Twisting-Engineered Hierarchical Structures of Hydrogels

The hierarchical architecture of natural muscle bundles and collagen fibers inspires our multi-scale twisted fiber design, where controlled torsional alignment mimics biological structural optimization (Figure 1a). This biomimetic approach enables progressive polymer chain organization across molecular to macroscopic scales, yielding fibers with exceptional mechanical performance, including enhanced toughness, strain tolerance, and shear strength (Figure 1b, c) [28, 29]. These twisted fibers are capable of bearing loads far beyond their own weight while maintaining structural integrity (Figure 1d). Compared to natural and synthetic soft materials, they occupy a previously unachieved region of high toughness and large stretchability, and exhibit superior overall mechanical performance across multiple criteria (Figure 1e,f) [11, 22, 23, 35–37]. Poly(vinyl alcohol) (PVA, 146–186 kDa, 99% hydrolyzed) serves as the model polymer due to its optimal hydrophilicity, established crystallinity control methodologies, and biocompatibility (Figure S1) [17, 38]. As detailed in Figure 2a, our fabrication protocol transforms initially disordered freeze-thawed hydrogel fibers [17] into twisting yet aligned architectures through sequential stretching, twisting and thermal annealing treatment. The hydrogel stretching was conducted through the classical drying in confined condition (termed as DCC) strategy, during which the polymer chain aligned along the stretching direction and forming nanofibrils structures [39]. Subsequent twisting treatment provides a spiral architecture of hydrogel fibre materials, and the structures were further locked through thermal annealing, where hydrogen bonds formed at the intra-/inter-fiber interface [38]. The resultant flexible fibers demonstrate remarkable load-bearing capacity, supporting weights exceeding 10 000 times their mass (100-g payload, Figure 1d). Systematic characterization via SEM and fluorescence imaging reveals the distinct surface texturization and periodic fibrillar packing patterns post-twisting (Figure 2b and Figure S2), while swelling tests confirm the preserved structural integrity (Figure 2c and Figure S3). Crystallinity analysis demonstrates progressive lattice refinement with alignment enhancement, where twisted fibers achieve minimized distance between adjacent crystalline domains (L = 12 nm) and maximum crystallinity (~35%) compared to alternative processing methods (Figure 2d and Figure S4). Small-angle X-ray diffraction patterns quantitatively validate this alignment-dependent crystallinity enhancement through intensified Bragg peak signatures (Figure S5). Axial stretching aligns polymer chains along the fiber axis, while torsional shear rotates them toward a helical direction (Figure S6a). This radially heterogeneous reorientation, with larger angles in the outer region (Figure S6b), agrees with the enhanced anisotropy observed in SAXS/WAXS and supports the formation of stable helical and highly crystalline structures.

Mechanical evaluation (Figure 2e,f and Figures S7 and S8) revealed fiber-number-dependent performance optimization, where stress–strain curves demonstrated synchronous improvement of tensile strength (σ_{max}) and elongation-at-break (ϵ) up to 4–200 fiber configurations. This regime exhibited maximum slope steepness in the linear elastic region, a critical indicator of

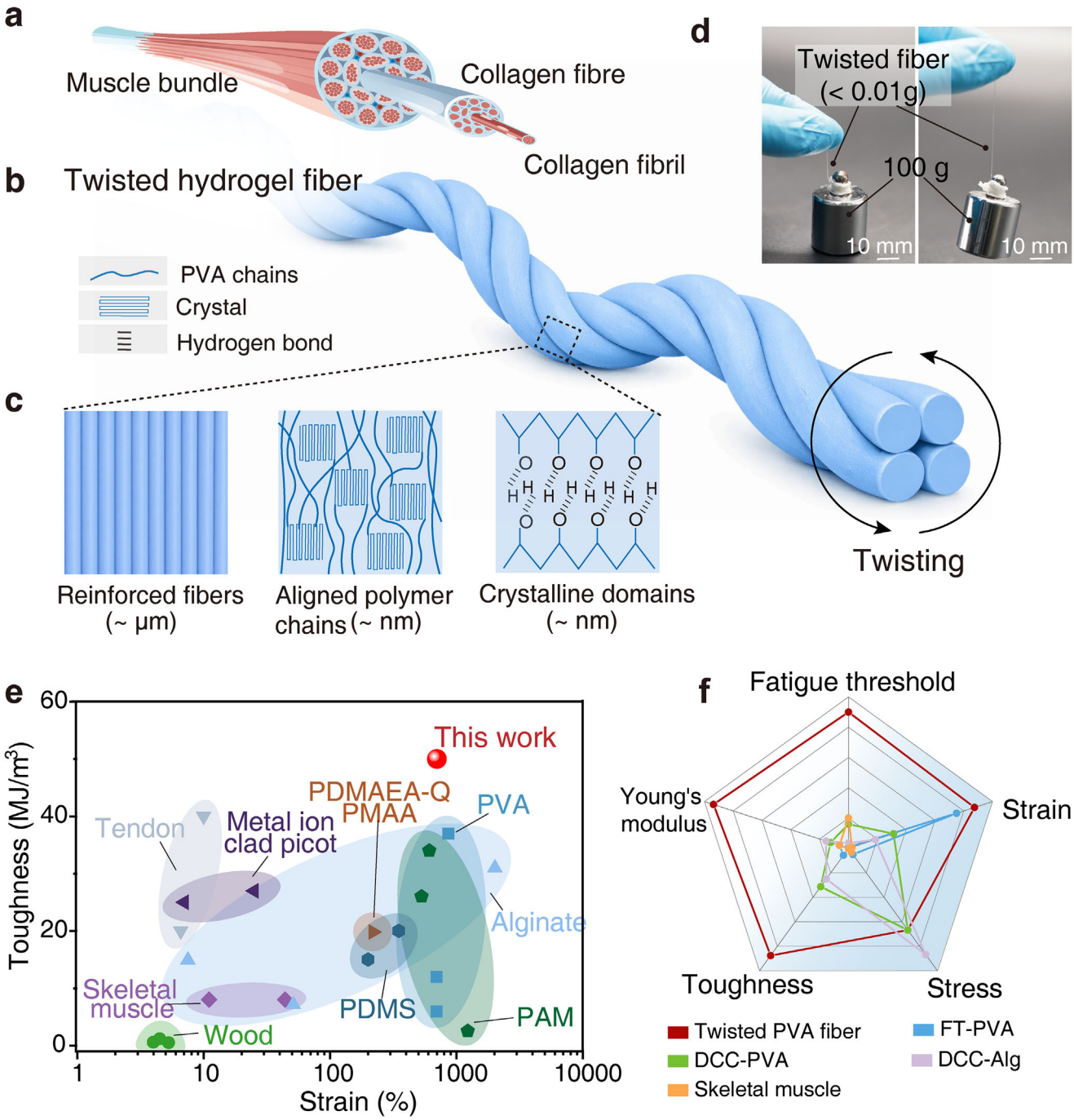

FIGURE 1 | | Fatigue-resistant hydrogel materials with bioinspired twisting architectures. (a) Schematic illustration of the hierarchical structure of muscles, ranging from the muscle bundles, collagen fibers, and collagen nanofibrils. (b,c)The bioinspired fabrication of fatigue resistant hydrogel fibers involving the twisting hydrogel fibers within one unit, and the structural hierarchy ranges from aligned polymer chains (sub-nanoscale), nanocrystals (nanoscale), polymer fibers (micoscale), and twisted fibers (micrometer- to millimeter-scale). Presence of nanoscale crystals and aligned fibril structures synergistically pin the crack, imparting them with astonished capability to resist fatigue cracks. (d) demonstrating the remarkably high strength of the twisted hydrogel fibers by sustaining a load (100 g) of 10 000× of its own weight. (e) Toughness-strain plot comparing twisted PVA hydrogel fibers with natural tissues (e.g., tendon, muscle, wood) and synthetic materials (e.g., PDMS, PVA, alginate, PAM) [11, 22, 23, 35–37]. (f) Radar chart of five mechanical properties, fatigue threshold, Young's modulus, strain, stress, and toughness, comparing twisted PVA fibers with control samples [9].

optimal load transfer efficiency. Beyond this threshold, σ_{max} continued its ascending trend while ϵ plateaued (~400%), with material toughness peaking at ~45 MJ m^{-3}. This performance ceiling is correlated to the interfacial saturation effects that constrain further energy dissipation enhancements [28, 33]. Collectively, these findings establish fiber-number modulation as a critical design parameter for balancing strength-elongation tradeoffs in hydrogel material systems. The elucidated processing-structure-property relationships provide a foundational framework for engineering twisted fiber assemblies with customized mechanical profiles, particularly suited for applications requiring long-term mechanical robustness.

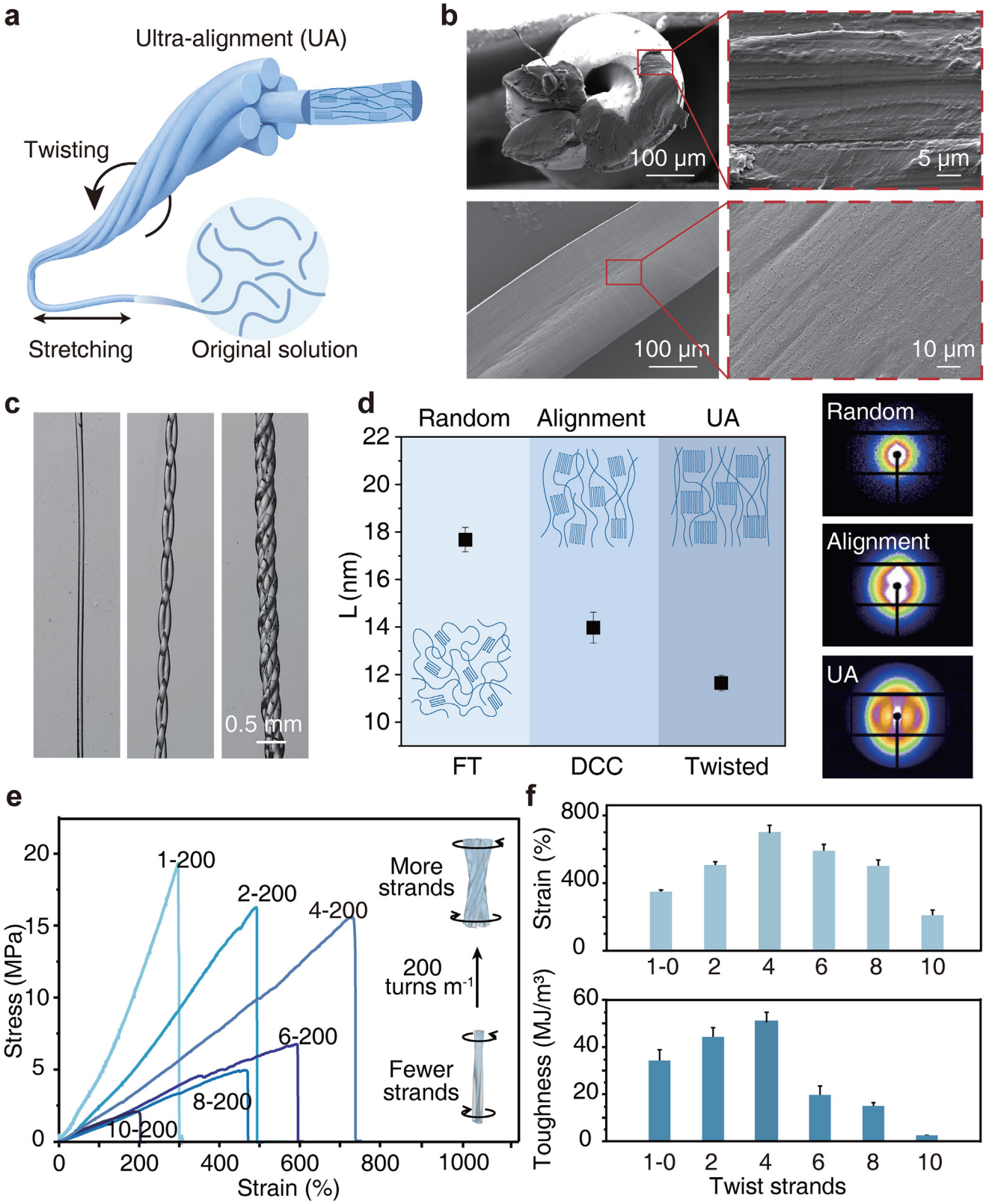

FIGURE 2 | | Hierarchical structures and mechanics of the twisted hydrogel fiber materials. (a) Schematic illustration of the hierarchical structure of the twisted hydrogel fiber materials. (b) Cross-sectional SEM images of the twisted hydrogel fiber materials. (c) Representative image of a single hydrogel fiber, and twisted hydrogel fibers with different twisting parameters. (d) Estimated averaged distance among crystals (L) for the hydrogel fiber materials from SAXS measurement, and the SAXS patterns of various hydrogel fiber samples. (e) Representative tensile stress–strain curves for the twisted hydrogel fiber materials with different twisting parameters. The first number indicates fiber count, and the second number (after the hyphen) represents twist density (turns m^{-1}). For example, 2–200 refers to 2 fibers with 200 turns m^{-1}. (f) Summary of the mechanical parameters, such as strain and toughness, of these twisted hydrogel fiber samples. Data in (d) and (f) are presented as means ± S.D., $n = 3$.

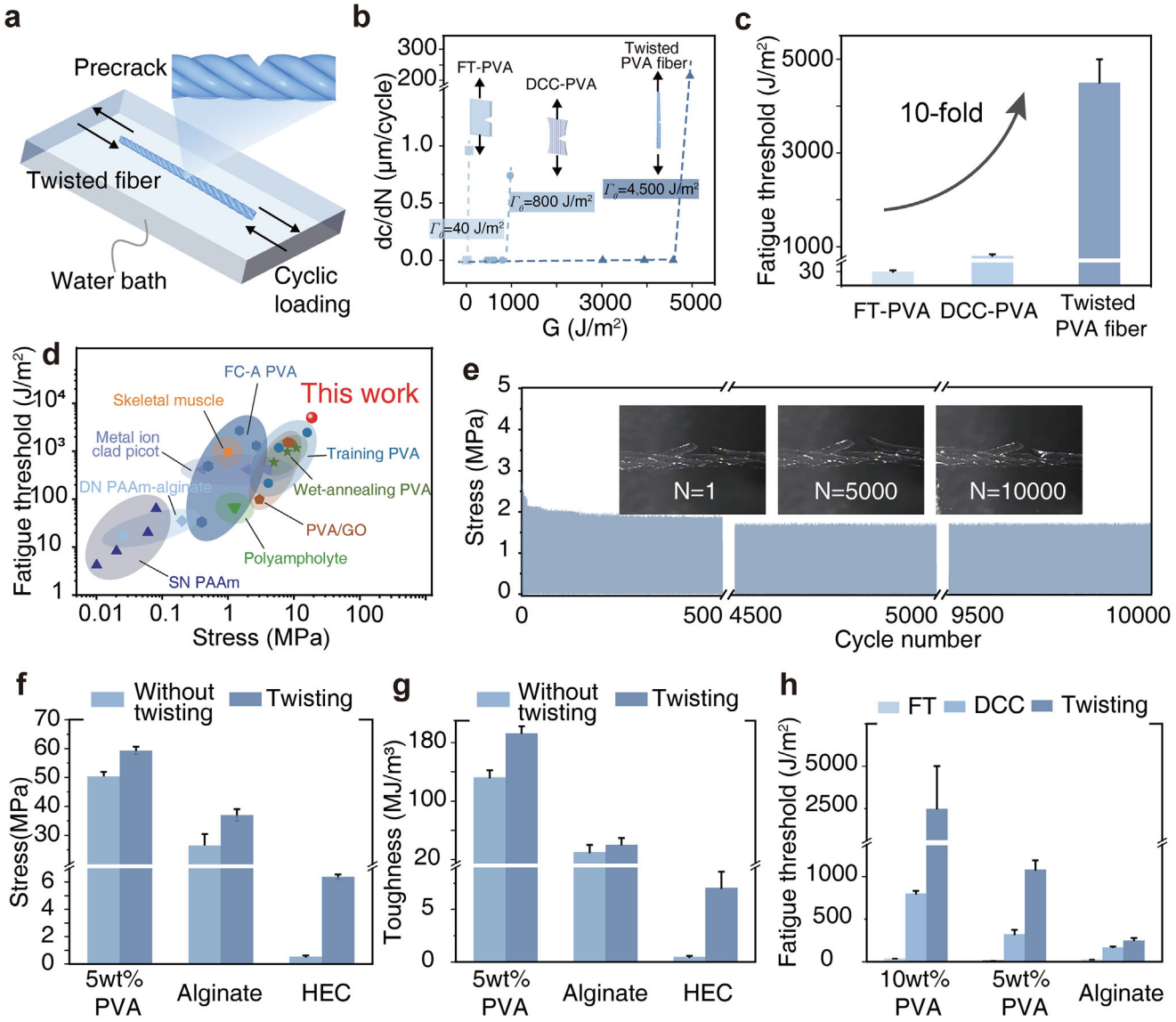

FIGURE 3 | | Fatigue resistance of the hydrogel fiber materials with twisting architectures. (a) Illustration of measuring the crack extension per cycle (dc/dN) against energy release rate G for various pre-notched hydrogel materials within a water bath, in order avoid the water lost of hydrogel materials during the mechanical test. (b) Plotting of the dc/dN vs. G for various hydrogel samples, including the FT-PVA, DCC-PVA, and twisted PVA fibers. Linear extrapolating the curve to intercept with the abscissa yields the critical energy release rate G_c, which is defined as the fatigue threshold (Γ_0) of the samples. (c) Summary of the quantified fatigue threshold (Γ_0) for the hydrogel samples. (d) Comparison chart by plotting the fatigue thresholds vs. strength among various mechanically robust hydrogel materials, including the polyampholyte hydrogels (100 J m^{-2}) [15], PVA/GO composites (1700 J m^{-2}) [2, 27], and biological tissues like skeletal muscle (~ 1000 J m^{-2}) [11, 17, 22, 23, 40]. (d,e) Validation of the estimated fatigue threshold of the twisted PVA hydrogel fiber sample by applied an energy release rate of 4500 J m^{-2} on a pre-cut sample for 10 000-cycle test. (f–h) Summary of tensile strength, toughness, and fatigue threshold (Γ_0) of twisted PVA fibers (5 or 10wt.%), alginate fibers and HEC fibers samples with the same twisting hierarchy, in order to validate the generality of our design and fabrication strategy. Data in (b), (c) and (f–h) are presented as means ± S.D., $n = 3$.

2.2 | Fatigue Resistance of Twisted Hydrogel Fibers

Comprehensive microstructural analysis demonstrates that multiscale structural optimization via torsional alignment substantially enhances the fatigue resistance of PVA hydrogel fibers. To further quantify the fatigue threshold of these hydrogel samples employing the single-notch method, by linearly plotting the crack extension per cycle (dc/dN) vs. energy release rate G and obtaining the critical energy release rate G_c as the fatigue threshold Γ_0 [17, 38]. As shown in Figure 3a, torsionally processed fibers exhibit fatigue crack propagation rates (dc/dN) reduced by 1–2 orders of magnitude compared to FT-PVA and DCC-PVA hydrogel counterparts across all energy release rates (G). This measurement reveals exceptional Γ_0 values exceeding 4500 J m^{-2}, representing 100-fold and 5-fold improvements over FT-PVA (40 J m^{-2}) and DCC-PVA (800 J m^{-2}) hydrogels, respectively(Figure 3b,c). The structural superiority originates from a hierarchical organization spanning molecular to micrometer scales, where torsional processing further improves the mechanical energy dissipation and crack tolerance (Figure S9). These features synergistically dissipate energy through cooperative

stress transfer between fibers, reduce local stress concentrations, and dissipate mechanical energy via inter-fiber friction during the deformation [34], enabling performance surpassing current hydrogel systems, including polyampholyte hydrogels (100 J m^{-2}) [15], PVA/GO composites (1700 J m^{-2}) [2, 27], and biological tissues like skeletal muscles (~1000 J m^{-2}) (Figure 3d) [11, 17, 22, 23, 40].

Cyclic loading tests confirm exceptional durability, over ~90% stress retention after 10 000 cycles (Figure 3e and Movie S1). The invariant stress–strain profiles under prolonged dynamic loading indicate minimal cumulative damage accumulation, a critical advantage for applications requiring long-term mechanical robustness in repetitive motion environments (e.g., load-bearing artificial muscles and soft robotics). These results establish twisted hydrogel fibers as prime candidates for high-durability applications, imparting conventional polymer networks with unprecedented fatigue resistance (<10^4 cycle stability).

Our torsion-induced chain alignment strategy provides a generalizable platform for enhancing the fatigue resistance of hydrogel systems and exhibits consistent performance improvements across diverse polymer matrices. For example, in 5 wt.% PVA fibers, torsional processing enhances ultimate tensile strength from 10 to 12 MPa (+120%) and toughness from 25 to 40 MJ m^{-3} (+160%) (Figure 3f,g and Figures S10 and S13). While for 10 wt.% PVA systems, fatigue thresholds increase from 800 to 4500 J m^{-2} post-twisting, surpassing most synthetic hydrogel benchmarks (Figure 3h). Our methodology's material-agnostic nature is further demonstrated in alginate fibers, where ultimate stress improves from 25 to 40 MPa, and fatigue thresholds from 25 to 250 J m^{-2} (Figures S11 and S14). Hydroxyethyl cellulose (HEC) fibers similarly show substantial enhancements, with ultimate stress increasing from 1 to 6 MPa and toughness from 1 to 6 MJ m^{-3} (Figure S12). This universal performance stems from programmable multiscale alignment that simultaneously optimizes the polymer chain alignment during the DCC process and energy dissipation through twisting geometry, enabling unprecedented fatigue resistance (Γ_0 <4500 J m^{-2}) while maintaining compositional flexibility essential for load-bearing applications.

2.3 | Underlying Mechanisms for Twist-Induced Improvement in Fatigue Resistance

This investigation establishes that the exceptional fatigue resistance of twisted hydrogel fibers originates from hierarchical structural ordering induced by torsional alignment, a phenomenon spanning nanoscale to mesoscale dimensions with pronounced geometric parameter sensitivity [28]. A multiscale computational framework (Figure 4a), implemented through LAMMPS simulations, employs dissipative particle dynamics (DPD) to systematically analyze behavior evolution during mechanical deformation [41]. Custom Python algorithms enable precise helical architecture construction (Figure 4b), ensuring geometric fidelity and thermodynamic equilibrium maintenance. The simulation protocol initiates with conjugate gradient-based energy minimization, subsequently transitioning to dynamic relaxation governed by a Berendsen thermostat. Interatomic interactions are modeled through harmonic potentials for bonded pairs and Lennard–Jones potentials for non-bonded systems, with parameters directly adopted from established force fields to preserve energetic-entropic balance [42]. Stress tensor analysis incorporating von Mises stress evaluation and integrated fracture criteria demonstrates that topological-geometric synergy governs mechanical robustness, a finding validated through open-source OVITO visualization [43].

The topological modification of stress fields in twisted architectures inhibits crack propagation via polymer chain alignment and helical ordering, with experimental and computational evidence identifying a critical reinforcement threshold at four helical turns. Four-turn configurations (4 fibers with 200 turns m^{-1}) at ca. 10% engineering strain exhibit optimal axial stress transfer (Figure 4c), while excessive twisting (e.g., ten turns, 10 fibers with 200 turns m^{-1}) disrupts stress redistribution (Figure 4d). This threshold is further corroborated by stress–strain curve congruence in strength, strain, and toughness metrics (Figure 4e). Geometric analysis reveals fundamental differences in rotational behavior: four-turn fibers display coherent cross-sectional rotation with uniformly increasing z-component values (5%–20% strain range, Figure 4f), whereas ten-turn counterparts exhibit alternating z-components (2%–8% strain, Figure 4g) indicative of counter-rotational failure mechanisms. Shear strain characterization demonstrates four-turn systems maintain uniform distributions (5%–25%, Figure 4h) with inter-fiber sliding (points a-b) and twisting (points c-d) revealed through Lagrangian analysis. Conversely, ten-turn configurations develop localized shear concentrations at ca. 9% strain (Figure 4i), featuring terminal cluster sliding (points e-f) and twisting (points g-h) that precipitate geometric locking and knotting phenomena (Movie S2).

2.4 | Bioinspired Actuator Engineered with Twisted Hydrogel Fibers

The introduction of twisting architecture into conventional hydrogel material systems (i.e. PVA, alginate or cellulose) could substantially improve their capability to resist fatigue crack propagation, making them potential candidates as load-bearing component of soft actuators, where long-term mechanical reliability and structural stability are critical to ensuring both device functionality and longevity. As shown in Figure 5, we design and fabricate a soft actuator, with its architecture biomimetically derived from the hierarchical organization of frog tongue musculature. The soft actuator is pneumatically driven through its compliant channels to achieve programmable shape morphing, while our twisted hydrogel fibers function as dual load-bearing and elastic recoil elements, efficiently storing mechanical energy during pneumatically-triggered deformation (Figure 5a,b and Figure S15). Upon pneumatic activation, axial extension occurs through channel expansion, while subsequent depressurization triggers spontaneous curling via prestrain-driven contraction (Figure 5c, Figure S16 and Movie S3). This cyclic actuation subjects the fibers to repetitive tensile-compressive loading, with interfacial stress concentrations localized at fiber-matrix junctions. Conventional soft actuators lacking reinforcement typically experience microcrack propagation and interfacial delamination within limited operational cycles, whereas our torsion-engineered alignment ensures exceptional structural integrity under prolonged operation.

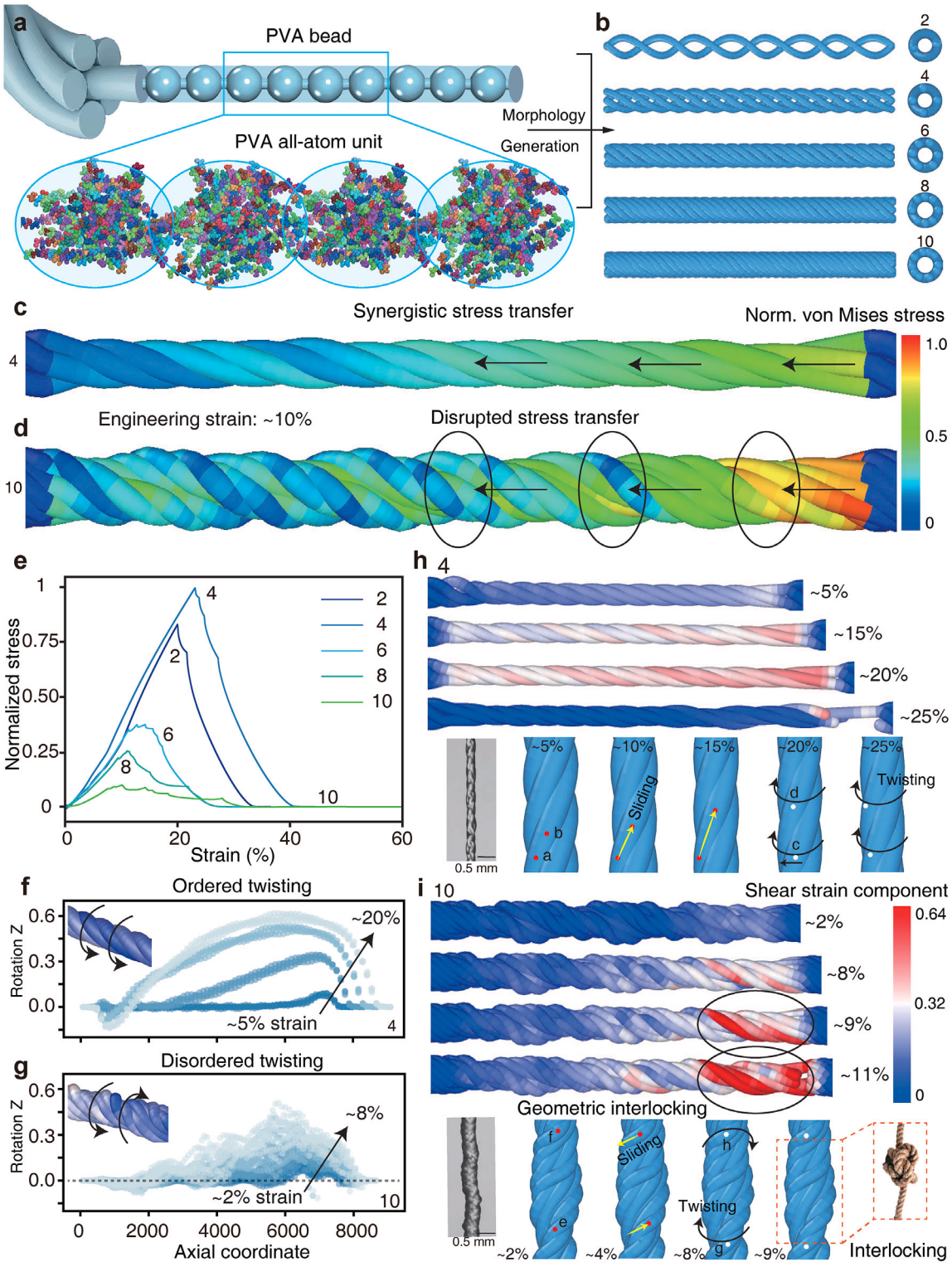

FIGURE 4 | | Multiscale analysis of topological and geometric effects on the twisted hydrogel fiber materials. (a) Schematic of the DPD-based cross-scale computational framework. (b) Helical fiber architectures generated via Python routines. (c) Normalized von Mises stress field for four-turn fibers at a ~10% engineering strain, revealing synergistic stress transfer. (d) Von Mises stress field for ten-turn fibers, revealing disrupted stress transfer. (e) Nonlinear DPD-simulated stress–strain curves for fibers with varying twist numbers, confirming a critical threshold of four turns through the evolution trends in strength, strain, and toughness. (f) For four-turn fibers (4 fibers with 200 turns m^{-1}), the z-component of the rotation vector increases uniformly with tensile strains (~5%–20%), indicating coherent cross-sectional rotation. (g) For ten-turn fibers (10 fibers with 200 turns m^{-1}), the z-component alternates with strains (~2%–8%), reflecting relative twisting between opposing sides of the cross-section. (h) In four-turn fibers, the shear strain distribution remains uniform over tensile strains of ~5%–25%, evidencing the inter-/intra-fiber sliding and twisting. (i) In ten-turn fibers at ~9% tensile strain, localized shear strain at cluster ends, combined with relative sliding and twisting, results in geometric locking and subsequent interlocking and knotting.

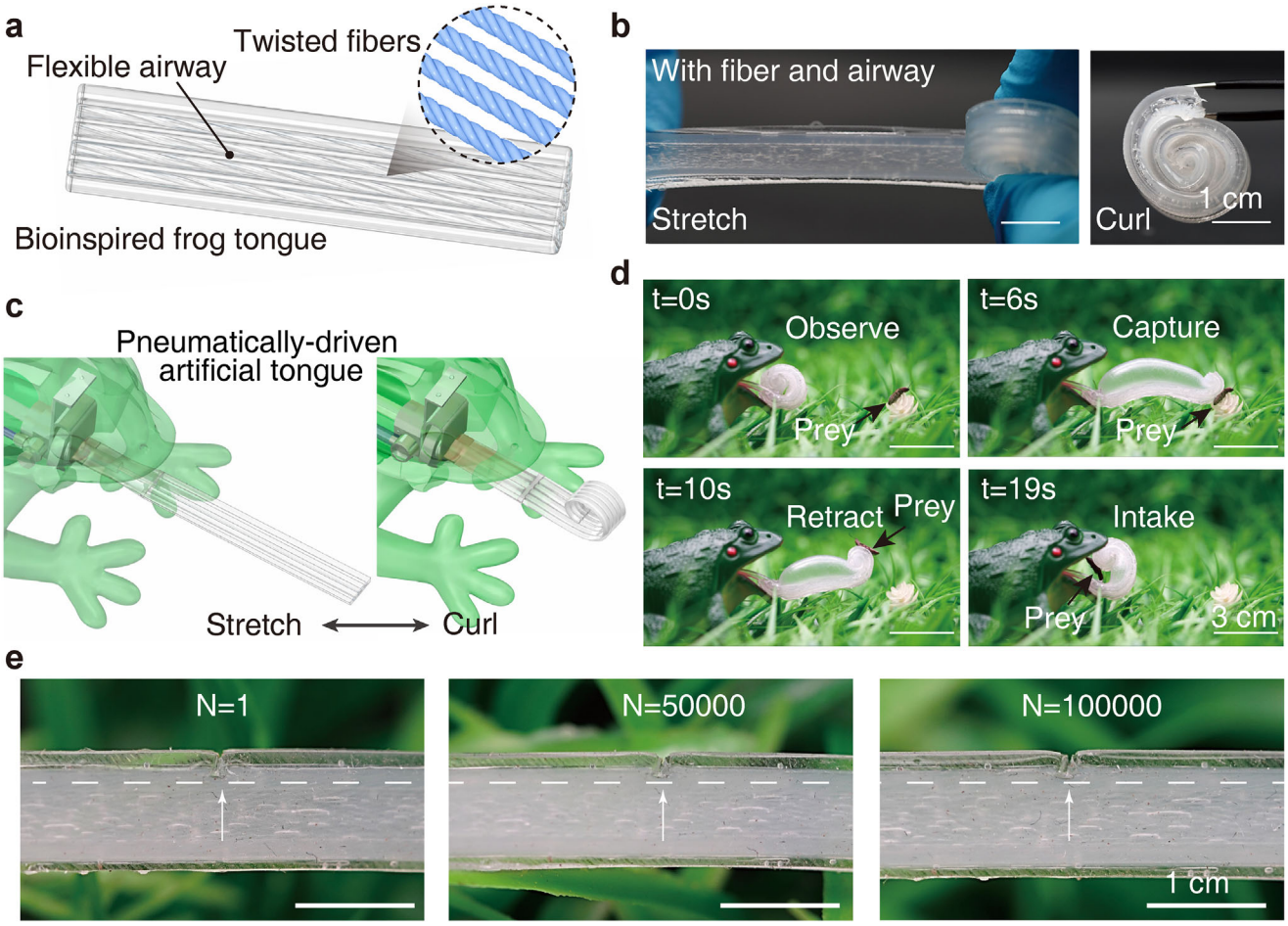

FIGURE 5 | | Functional demonstration as the load-bearing components within a frog tongue-like actuator. (a) Schematic illustration of the geometry of a tongue-like actuator, incorporating the twisted hydrogel fibers as the load bearing components, while airways as the pneumatical actuation channel. (b) Image of the as-fabricated soft actuator, as well as the stretching/curling of the tongue-like actuator through pneumatical actuation. Scale bar: 1cm. (c) Schematic illustration of the frog-like robot with the pneumatically-driven artificial tongue. (d) Snapshot images of the trajectory of the frog-like robot's capability for capturing a prey. The tongue is experiencing stretching through pneumatical actuation, capturing the prey, contracting and intaking of the prey within 20 s. Scale bar: 3 cm. Frog-like robot (commercial outer shell) purchased via Taobao (online marketplace, China). Image courtesy of the authors. (e) Image of the pre-cracked (1/5 of the overall width) artificial tongue before and after 100 000-cycle prolonged deformation (~ 500 h). Scale bar: 1 cm.

As demonstrated in Figure 5e, the artificial frog tongue maintains its pristine structural continuity through 50 000–100 000 actuation cycles, exhibiting no detectable cracking, delamination, or interfacial separation when comparing initial (N = 1) and terminal (N = 100 000) states. Post-cycling microstructural analysis reveals preserved fiber alignment and dense packing architecture, a critical advantage over homogeneous hydrogel counterparts that typically fail within < 10 000 cycles. Functional evaluation confirms consistent actuation performance, with enhanced response kinetics (with activation time reduced by approximately 60%) and curling compactness (with curvature radius reduced by approximately 40%) compared to non-reinforced systems. The biomimetic validation in Figure 5d, with photographs taken by the authors, demonstrates full replication of biological prey capture dynamics, target identification, rapid capture, controlled retraction, and payload transfer, over multiple operational cycles (Movie S4), confirming the system-level reliability.

3 | Conclusions and Perspectives

This study establishes torsion-induced multiscale alignment as a universal strategy for engineering fatigue-resistant hydrogel fibers with unprecedented fatigue resistance. Through hierarchical structural organization spanning molecular chains to macroscopic fibrillar architectures, we demonstrate synergistic enhancement of toughness (150% enhancement), stretchability (200% strain), and fatigue resistance (1000% enhancement) across chemically diverse hydrogel systems. The torsion-aligned PVA system exhibits exceptional mechanical durability, featuring a record fatigue threshold exceeding 4,500 J m^{-2} and stable operation through over 10^4 dynamic loading cycles, with properties surpassing conventional hydrogel benchmarks by 1-2 orders of magnitude. The methodology's material-agnostic efficacy is validated through alginate and hydroxyethyl cellulose systems, where fibrillar alignment and twisting architecture enable three- to five-fold improvement in fatigue threshold. Mechanistically

inspired by the collagen/tendon biomechanics, this architecture facilitates multiscale energy dissipation through reversible hydrogen bond rupture and controlled fibril sliding, thus effectively addressing the persistent challenge of hydrogel fatigue failure. Functional validation is achieved through a biomimetic actuator replicating frog tongue prototypes, capable of rapid reversible motion (<100 000 cycles) with preserved structural integrity. This work bridges critical gaps in hydrogel engineering, enabling durable soft material systems for demanding applications, such as artificial muscles, load-bearing implants, and adaptive robotics, where conventional hydrogels are prone to fatigue failure. failed due to cyclic degradation. Beyond soft actuation, the combination of tissue-like compliance, high cyclic durability, and fibrous geometry positions this platform as a promising candidate for bio-integrated applications, including artificial tendons and ligaments, surgical sutures, and mechanically robust implantable interfaces [7, 18, 25]. More broadly, fiber twisting offers a scalable route to bridge the gap between laboratory hydrogel mechanics and the long-term reliability required for functional biomedical and soft robotic systems.

4 | Experimental Section

4.1 | Fabrication of Twisted PVA Hydrogel Fibers

The poly(vinyl alcohol) (PVA) hydrogel fibers were synthesized via a template-assisted hierarchical alignment protocol. A 10 wt.% PVA aqueous solution was thermally homogenized at 90°C for 2 h to ensure complete dissolution. The viscous precursor was subsequently transferred into a polydimethylsiloxane (PDMS) tubular mold (inner diameter: 0.25 mm), with rigorous visual inspection to eliminate air bubble formation. The samples were then subjected to three programmed cryogenic cycles (–20°C for 12 h and 25°C for 4 h) to induce physical crosslinking through phase-seperation and nanocrystal formation. After that, the nascent hydrogel fibers were demolded and subjected to drying in confined condition [39]. Specifically, the hydrogel fibers were uniaxially stretching at 100% strain under 90% relative humidity for 24 h, during which the process the polymer chains oriented along the length direction and forming nanofibrils. The dehydrated fibers were then re-equilibrated in deionized water (24 h, 25°C) to restore hydrogel plasticity, followed by torsional processing with a twisting apparatus at specific twisting parameters. Upon drying in air for 24 h at the twisted state, the fiber bundles were then thermally annealed at 90°C, in order to lock in the helical microstructure through interfacial hydrogen bonding. This sequential alignment strategy, combining tensile stretching and torsional shear, enabled multiscale structural ordering from molecular chains (nanoscale alignment) to macroscopic fibrillar bundles (microscale helical pitch).

4.2 | Fatigue Threshold Measurement

The fatigue thresholds of the hydrogel samples were quantified through the classical single-notch method [17, 38]. Different from those methods used to introduce pre-crack in hydrogel film sample, we simply cut one single fiber fo the twisted fiber bundles, and cyclic tensile tests were performed under a predesignated strain. The hydrogel fibers were fixed onto cardboard to ensure stability during testing, in order to prevent slipping. The notch was placed at the center of the twisted fiber sampels. Cyclic tensile tests were conducted using a mechanical stretcher (Cellscale) on both notched and unnotched hydrogel fiber samples. Crack length changes were monitored in each cycle using a digital microscope.

For unnotched samples, the same strain was applied. Strain energy density for each cycle was calculated by integrating stress over the deformation range. For the notched fibers, energy release rate was calculated in each cycle based on the applied strain and fiber deformation. By varying the applied strain, a plot of crack growth rate dc/dN vs. energy release rate G was generated. The fatigue threshold was determined by linearly extrapolating the crack growth rate vs. energy release rate curve to its intersection with the x-axis. To verify the accuracy of the extrapolated energy release rate (Γ_0), notched hydrogel fibers were tested at the estimated energy release rate for 10 000 cycles. Crack propagation was continuously monitored with a camera to confirm that the extrapolated energy release rate matched the actual fatigue threshold of the samples.

4.3 | The Methodological Framework of Dissipative Particle Dynamics

In this work, all simulations were carried out in LAMMPS by first reading the polymer configuration from a data file and defining the harmonic bond and angle potentials $U_{\text{unbonded}} = K_{\text{bond}}\,(r - r_0)^2 + K_{\text{angle}}\,(\theta - \theta_0)^2$ together with a Lennard–Jones nonbonded interaction $U_{ij}\left(r, d_{\text{bead}}\right) = \varepsilon(d_{\text{bead}})[(\sigma(d_{\text{bead}})/r)^{12} - (\sigma(d_{\text{bead}})/r)^6]$. The system was energy-minimized via a conjugate-gradient algorithm, then equilibrated under NVE dynamics coupled to a Berendsen thermostat, with two end regions held fixed as grips and the central region free to move. After resetting the timestep, uniaxial tension was applied by driving the grips apart at constant velocity while continuing NVE integration with thermostatting. During deformation, we recorded per-atom stresses (including von Mises), the global stress–strain curve, and trajectory snapshots at regular intervals; the final deformed configuration was written out for subsequent analysis.

4.4 | Frog Tongue-Inspired Actuator

The biomimetic actuator fabrication protocol involves three critical stages: fiber encapsulation, shape programming, and actuation integration. Pre-stretched twisted hydrogel fibers are embedded within an Ecoflex precursor under vacuum to eliminate interfacial voids, followed by room-temperature curing to secure fiber-matrix integration. Differential shrinkage between the hydrogel fibers and matrix induces spontaneous curvature matching the frog's tongue morphology (radius: 1 cm). Actuation is mediated by an embedded pneumatic network comprising silicone microchannels (diameter: 400 μm) connected to a pressure-regulated air dispenser (0–300 kPa). The actuator is then assembled into the shell of a commercially available frog-like toy, purchased via Taobao (online marketplace, China). The actuation system allows precise control of the rapid extension and curling of the tongue, simulating the prey-catching action of the frog's tongue. Cyclic pressurization (0.2 Hz frequency)

generates reversible extension-retraction kinematics (max strain: 200%), with motion fidelity validated against biological benchmarks using high-speed videography. Accelerated 10 000-cycle fatigue testing was conducted to confirm structural integrity over prolonged use, with no detectable cracks or delamination observed post-cycling, demonstrating exceptional durability for repetitive motion applications.

4.5 | Statistical Analysis

All results are presented as mean ± standard deviation (S.D.). Unless otherwise stated, each experiment was independently repeated at least three times, and each condition was measured in triplicate (n = 3). No data transformation or normalization was applied unless explicitly stated, and no data points were excluded as outliers unless justified. No hypothesis testing was performed in this study; therefore, no p values are reported. Data processing and plotting were performed using Origin 8.0 (OriginLab, Northampton, MA, USA). All mesoscale simulations in this work were performed using the Large-scale Atomic/Molecular Massively Parallel Simulator (LAMMPS).

Acknowledgments

The authors acknowledged the financial support from the National Key R&D Program of China (2024YFA0920100), National Natural Science Foundation of China (52373139 and U2436202), Guangdong Basic and Applied Basic Research Foundation (2024A1515240042), International Science and Technology Cooperation Programs of Guangdong Province (2025A0505020003), Basic Research Program of Shenzhen (JCYJ20230807093419041 and JCYJ20240813094159001). The authors also gratefully acknowledge the support from the Shenzhen Science and Technology Innovation Commission (KJZD20240903101400001) and the Development and Reform Commission of Shenzhen Municipality (XMHT20240115003). The authors would also like to acknowledge the technical support from SUSTech Core Research Facilities.

Conflicts of Interest

The authors declare no conflicts of interest.

Data Availability Statement

The data that support the findings of this study are available from the corresponding author upon reasonable request.

References

1. C. Zhao, J. Park, S. E. Root, and Z. Bao, "Skin-Inspired Soft Bioelectronic Materials, Devices and Systems," *Nature Reviews Bioengineering* 2, no. 8 (2024): 671–690.

2. X. Liang, G. Chen, S. Lin, et al., "Anisotropically Fatigue-Resistant Hydrogels," *Advanced Materials* 33, no. 30 (2021): 2102011.

3. X. Chen, F. Liu, Q. Yu, M. Yang, Z. Suo, and J. Tang, "A Soft and Fatigue-Resistant Material That Mimics Heart Valves," *Matter* 8, no. 2 (2025): 101926.

4. J. Liu, S. Lin, X. Liu, et al., "Fatigue-Resistant Adhesion of Hydrogels," *Nature Communications* 11, no. 1 (2020): 1071.

5. X. Chen, Y. Feng, P. Zhang, Z. Ni, Y. Xue, and J. Liu, "Hydrogel Fibers-Based Biointerfacing," *Advanced Materials* 37, no. 4 (2025): 2413476.

6. X. Liu, C. Steiger, S. Lin, et al., "Ingestible Hydrogel Device," *Nature Communications* 10, no. 1 (2019): 493.

7. K. Wen, C. Zhang, G. Zhang, et al., "Jellyfish-Inspired Artificial Spider Silk for Luminous Surgical Sutures," *Advanced Materials* 36, no. 36 (2024): 2314158.

8. X. Liu, J. Liu, S. Lin, and X. Zhao, "Hydrogel Machines," *Materials Today* 36 (2020): 102–124.

9. X. Li and J. P. Gong, "Design Principles for Strong and Tough Hydrogels," *Nature Reviews Materials* 9, no. 6 (2024): 380–398.

10. J. Tang, J. Li, J. J. Vlassak, and Z. Suo, "Fatigue Fracture of Hydrogels," *Extreme Mechanics Letters* 10 (2017): 24–31.

11. X. Liu, S. Rao, W. Chen, et al., "Fatigue-Resistant Hydrogel Optical Fibers Enable Peripheral Nerve Optogenetics During Locomotion," *Nature Methods* 20, no. 11 (2023): 1802–1809.

12. Z. Zhang, G. Chen, Y. Xue, et al., "Fatigue-Resistant Conducting Polymer Hydrogels as Strain Sensor for Underwater Robotics," *Advanced Functional Materials* 33, no. 42 (2023): 2305705.

13. N. Park, Z. Fan, and J. Kim, "Hierarchical Tough Hydrogel with Enhanced Rigidity and Extensibility for Strain Sensing, Posture Guide, and Injury-Prevention," *Advanced Functional Materials* 35, no. 17 (2025): 2419830.

14. Y. Tan, R. Liao, Y. Mu, et al., "Hierarchically-Structured and Mechanically-Robust Hydrogel Electrolytes for Flexible Zinc-Iodine Batteries," *Advanced Functional Materials* 34, no. 45 (2024): 2407050.

15. X. Li, K. Cui, T. L. Sun, et al., "Mesoscale Bicontinuous Networks in Self-Healing Hydrogels Delay Fatigue Fracture," *Proceedings of the National Academy of Sciences* 117, no. 14 (2020): 7606–7612.

16. X. Li, K. Cui, T. Kurokawa, et al., "Effect of Mesoscale Phase Contrast on Fatigue-Delaying Behavior of Self-Healing Hydrogels," *Science Advances* 7, no. 16 (2021): eabe8210.

17. S. Lin, J. Liu, X. Liu, and X. Zhao, "Muscle-Like Fatigue-Resistant Hydrogels by Mechanical Training," *Proceedings of the National Academy of Sciences* 116, no. 21 (2019): 10244–10249.

18. Y. Tang, B. Wu, J. Li, C. Lu, J. Wu, and R. Xiong, "Biomimetic Structural Hydrogels Reinforced by Gradient Twisted Plywood Architectures," *Advanced Materials* 37, no. 1 (2025): 2411372.

19. Y. Tang, C. Lu, and R. Xiong, "Biomimetic Mechanically Robust Chiroptical Hydrogel Enabled by Hierarchical Bouligand Structure Engineering," *ACS Nano* 18, no. 22 (2024): 14629–14639.

20. J. Kim, G. Zhang, M. Shi, and Z. Suo, "Fracture, Fatigue, and Friction of Polymers in Which Entanglements Greatly Outnumber Cross-Links," *Science* 374, no. 6564 (2021): 212–216.

21. H. Lei, L. Dong, Y. Li, et al., "Stretchable Hydrogels with Low Hysteresis and Anti-Fatigue Fracture Based on Polyprotein Cross-Linkers," *Nature Communications* 11, no. 1 (2020): 4032.

22. B. Xue, Z. Bashir, Y. Guo, et al., "Strong, Tough, Rapid-Recovery, and Fatigue-Resistant Hydrogels Made of Picot Peptide Fibres," *Nature Communications* 14, no. 1 (2023): 2583.

23. M. Hua, S. Wu, Y. Ma, et al., "Strong Tough Hydrogels via the Synergy of Freeze-Casting and Salting Out," *Nature* 590, no. 7847 (2021): 594–599.

24. Y. Feng, L. Shan, Y. Wang, X. Chen, C. Wang, and J. Liu, "Conductive Hydrogels with Topographical Geometry and Mechanical Robustness for Enhanced Peripheral Nerve Regeneration," *ACS Nano* 19, no. 17 (2025): 16675–16684.

25. N. Park and J. Kim, "Anisotropic Hydrogels with a Multiscale Hierarchical Structure Exhibiting High Strength and Toughness for Mimicking Tendons," *ACS Applied Materials and Interfaces* 14, no. 3 (2021): 4479–4489.

26. X. Liang, G. Chen, I. M. Lei, et al., "Impact-Resistant Hydrogels by Harnessing 2D Hierarchical Structures," *Advanced Materials* 35, no. 1 (2023): 2207587.

27. X. Liang, G. Chen, S. Lin, et al., "Bioinspired 2D Isotropically Fatigue-Resistant Hydrogels," *Advanced Materials* 34, no. 8 (2022): 2107106.

28. X. Zhou, S. Fang, X. Leng, Z. Liu, and R. H. Baughman, "The Power of Fiber Twist," *Accounts of Chemical Research* 54, no. 11 (2021): 2624–2636.

29. K. Zhang, X. Shi, H. Jiang, et al., "Design and Fabrication of Wearable Electronic Textiles Using Twisted Fiber-Based Threads," *Nature Protocols* 19, no. 5 (2024): 1557–1589.

30. Y. Xiao, G. Mei, D. Feng, et al., "Elastocaloric Heat Pump by Twist Induced Periodical Non-Linear Stress for Low Hysteresis and High Carnot Efficiency," *Advanced Materials* 36, no. 46 (2024): 2407009.

31. Z. Zhang, B. Cui, Y. Sun, et al., "Biomimetic Gradual Helical Structure for Enhancing the Strength and Toughness of Fiber-Reinforced Composites," *Advanced Materials* 37 (2025): 2501166.

32. Y. Dou, Z.-P. Wang, W. He, et al., "Artificial Spider Silk from Ion-Doped and Twisted Core-Sheath Hydrogel Fibres," *Nature Communications* 10, no. 1 (2019): 5293.

33. K. Yu, C. Li, W. Gu, et al., "High-Strength Cellulose Fibres Enabled by Molecular Packing," *Nature Sustainability* 8 (2025): 411–421.

34. J. Fu, Y. Li, T. Zhou, et al., "Large Stroke Radially Oriented MXene Composite Fiber Tensile Artificial Muscles," *Science Advances* 11, no. 2 (2025): eadt1560.

35. H.-L. Gao, R. Zhao, C. Cui, et al., "Bioinspired Hierarchical Helical Nanocomposite Macrofibers Based on Bacterial Cellulose Nanofibers," *National Science Review* 7, no. 1 (2020): 73–83.

36. S. Zhu, S. Wang, Y. Huang, et al., "Bioinspired Structural Hydrogels with Highly Ordered Hierarchical Orientations by Flow-Induced Alignment of Nanofibrils," *Nature Communications* 15, no. 1 (2024): 118.

37. Y. Shi, B. Wu, S. Sun, and P. Wu, "Aqueous Spinning of Robust, Self-Healable, and Crack-Resistant Hydrogel Microfibers Enabled by Hydrogen Bond Nanoconfinement," *Nature Communications* 14, no. 1 (2023): 1370.

38. S. Lin, X. Liu, J. Liu, et al., "Anti-Fatigue-Fracture Hydrogels," *Science Advances* 5, no. 1 (2019): eaau8528.

39. M. T. I. Mredha, Y. Z. Guo, T. Nonoyama, T. Nakajima, T. Kurokawa, and J. P. Gong, "A Facile Method to Fabricate Anisotropic Hydrogels with Perfectly Aligned Hierarchical Fibrous Structures," *Advanced Materials* 30, no. 9 (2018): 1704937.

40. E. Zhang, R. Bai, X. P. Morelle, and Z. Suo, "Fatigue Fracture of Nearly Elastic Hydrogels," *Soft Matter* 14, no. 18 (2018): 3563–3571.

41. S. Plimpton, "Fast Parallel Algorithms for Short-Range Molecular Dynamics," *Journal of Computational Physics* 117, no. 1 (1995): 1–19.

42. H. J. Risselada, "Martini 3: A Coarse-Grained Force Field with an Eye for Atomic Detail," *Nature Methods* 18, no. 4 (2021): 342–343.

43. A. Stukowski, "Visualization and Analysis of Atomistic Simulation Data with Ovito–The Open Visualization Tool," *Modelling and Simulation in Materials Science and Engineering* 18, no. 1 (2009): 015012.

Supporting Information

Additional supporting information can be found online in the Supporting Information section.

Supporting File: adma72589-sup-0001-SuppMat.pdf.

Supporting File: adma72589-sup-0002-MovieS2.mp4.

Supporting File: adma72589-sup-0003-MovieS3.mp4.

Supporting File: adma72589-sup-0004-MovieS4.mp4.

Supporting File: adma72589-sup-0005-MovieS5.mp4.